Construction and Building Materials 304 (2021) 124469

Contents lists available at ScienceDirect

Construction and Building Materials

journal homepage: www.elsevier.com/locate/conbuildmat

Improving ductility and bending features of poplar glued laminated beams by means of embedded carbon material

Francisco J. Rescalvo [a,*], Cristian Timbolmas [b], Rafael Bravo [b], Ignacio Valverde-Palacios [a], Antolino Gallego [a]

[a] Building Engineering School. University of Granada. Campus de Fuentenueva s/n, 18071 Granada, Spain
[b] Department of Structural Mechanics. University of Granada. Campus de Fuentenueva s/n, 18071 Granada, Spain

ARTICLE INFO

Keywords:
Timber
Glulam
Poplar
Composites
Ductility

ABSTRACT

Timber from fast-growing plantations such as poplar, typically used for plywood, can play a very important role in the coming decades for the development of a bio-economy. Long-term decarbonization in the construction sector depends to a considerable extent on the development of new engineered wood products for structural use. Composite materials resulting from the combination of materials with low mechanical properties (poplar timber) and materials with high mechanical properties in low proportions (carbon composites) stand as a good technological solution, in that they can provide low-weight products with competitive mechanical properties. This paper describes an experimental campaign involving glued laminated beams made of poplar timber and carbon composite material. Two types of carbon composites (fabric and pultruted laminated), thickness and location (at tension, compression or both sides) are studied in terms of ductility, stiffness and strength of the whole element by means of bending and non-destructive tests. The results demonstrate that the position and the type of reinforcement along the cross-section bear a clear influence on the mechanical behavior of the whole element. In terms of stiffness and strength, respective improvements of up to 44% and 33% are achieved. Moreover, high ductility values are obtained when the reinforcement is placed at the tension area, whereas britle behavior is observed when the reinforcement is placed only at the compression zone.

1. Introduction

One of the first structures with glued laminated beams (glulam) still in use today was built at the end of the 19th century: the assembly room of King Edward VI College in Southampton, England. The Technological Revolution and the development of a fully water-resistant phenol-resorcinol adhesive in 1942 gave rise to the glulam industry. Nowadays, the use of automatic finger-jointing and computer-controlled fabrication machines makes it possible to build highly demanding structures with extraordinary shapes and spans, and with a high degree of precision. Glulam beams pertain to what is currently known as Engineered Wood Products (EWP) [1].

Such improvements within the manufacturing proccess lead to more efficient use —hence conservation— of our timber resources, as wood species with lower diameters can be used. The FAO established that by 2020, 44% of the world's forests should be cultivated forests; and by 2050 some 75% of the wood used for industrial purposes should come from fast-growing plantations.

Poplar can be seen as a very suitable source of raw material for the elaboration of glulam beams. Given the currently predominant use of poplar for plywood around Europe, the P. × euroamericana hybrid I-214 cultivar is the most extensive species in poplar plantantions. According to FAO, in 2016 this cultivar covered about 145,000 ha, thus representing more than 50% of the total plantation area in Europe.

Mechanically, poplar timber (and particularly the clone-124) has an acceptable bending strength, yet a low modulus of elasticity. Therefore, the use of new materials such as reinforced fibre composites (FRP) serves to enhance stiffness —equaling or even surpassing engineering products based on other timber species. The notion of enhancing the mechanical properties of a glulam beam by means of FRP first appeared in the 1970s [2]. FRP reinforcement can be placed externally (Near Surface Mounted - NSM) or embedded [3]. The latter, despite requiring a more complicated elaboration process, is hidden, so that the aesthetic result is ideal for buildings where the timber is visible.

* Corresponding author.
E-mail address: rescalvo@ugr.es (F.J. Rescalvo).

https://doi.org/10.1016/j.conbuildmat.2021.124469
Received 13 January 2021; Received in revised form 28 July 2021; Accepted 4 August 2021
Available online 3 September 2021

One positive aspect of embedding reinforcement in the structural element is the consequent improvement in terms of fire resistance. Martin and Tingley reported that fire performance can be improved by placing the FRP internally, as the wood insulates the FRP, thus delaying the polymer matrix in reaching its glass transition temperature [4]. Williamson showed by experimental testing that a one-hour fire resistance rating can be obtained with larger size FRP-reinforced glulam beams even when no sacrificial lamination is included [5]

Several authors have worked with the reinforcement of different FRP layouts and wood species in glulam beams [6–9]. Ribeiro et al [10] strengthened glulam beams made of maritime pine wood, with a Modulus of Elasticity (MoE) similar to that of poplar. The application of a glass FRP (GFRP) pultruded lamella at the outer part of the tension side resulted in respective improvements of 46% and 41% for MoE and MoR (Module of Rupture). Other studies [11] found that the placement of two layers of GFRP fabric instead of one layer on the bottom side of a poplar glulam beam led to an improved MoE, from 7% to 13%. These works evaluated the effect of reinforcement applied near the neutral axis, where increases were slightly reduced. Nevertheless, all the fabric-reinforced beams showed ductile behaviour. Yang et al [12] studied several embedded reinforcement layouts by means of GFRP bars, steel bars and GFRP and CFRP (carbon FRP) plates placed at tension and compression zones in Douglas fir glulam beams. In the case of a CFRP layer placed at the tension side, they reported improvements of 1.3% and 21% for stiffness (relation between MoE and inertia) and ultimate moment, respectively. They also found that the placement of one GFRP layer at the bottom side led to a 2.3% decrease in stiffness, while its placement at the tension and compression side gave an enhancement value of up to 0.5%.

Ductility is a fundamental feature of structural elements such as bending resistance, MoR, and MoE [12–14]. Ductility can be defined as the ability to undergo significant plastic deformation before the rupture or breaking that corresponds to the failure of the element. Defomations can be understood to mean deflections, curvature or strains. Jorissen et al [15] evaluated plastic behavior by means of displacement and curvature ductility. In general, ductile behavior can be interpreted as an alarm before a catastrophic collapse.

In this work, poplar glulam beams internally reinforced with FRP were manufactured and tested so as to appraise the mechanical properties of the poplar I-214 low-grade species. Several layouts were analyzed and compared in terms of mechanical features. The fabric or pultruded lamella of CFRP —placed at the tension, compression, or both sides of the beam— were evaluated. The paper also provides an in-depth analysis of the ductile behavior, which is known to be a key indicator of both the engineering design and the safety of a buildińgs structural integrity.

2. Materials and methods

2.1. Poplar planks

All timber was extracted from a 9-year-old poplar plantation of the cultivar I-214 (Populus × euroamericana [Dode] Guinier) located nearby the city of Granada, Spain. Two logs measuring 2.5 m in length of each tree were used for this work. From them, planks sized 35 × 75 × 2000 mm were sawed and dried under natural conditions of good ventilation, protected from rain and direct solar radiation, during 6 months. After drying, the average Moisture Content (MC) was 10 ± 2%. All the planks were subjected to longitudinal acoustic resonance tests as described in [16] to arrive at the dynamic MoE, which was corrected to MC = 12% following the [UNE384] standard, then fitted to a normal distribution (see Fig. 1). The mean value was 7061 MPa, corresponding to class T8 class according the standard [17]. Standard deviation was 821 MPa. In order to avoid, as much as possible, heterogeneity of the manufactured glulam beams, only the planks within the standard deviation interval [6240–7882] were used (as seen between the green dotted lines in Fig. 1).

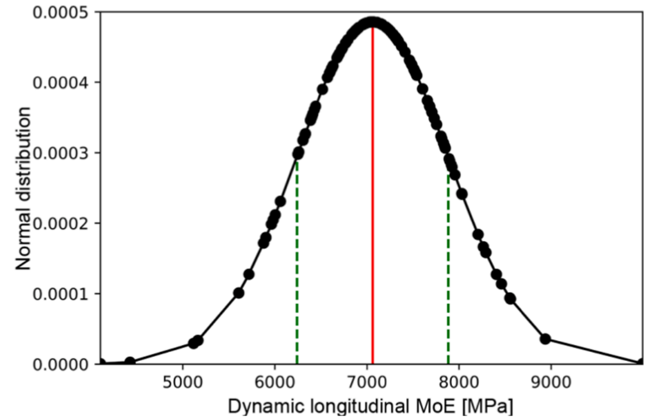

Fig. 1. Normal distribution of the dynamic longitudinal MoE of the sawed planks. Red line: Mean value. Green dotted line: Standard deviation limits. (For interpretation of the references to colour in this figure legend, the reader is referred to the web version of this article.)

2.2. FRP material

Two types of carbon fiber reinforced materials (CFRP) were used: i) Unidirectional pultruded CFRP plate Carboplate® E200; and ii) Unidirectional fabric Mapewrap® C Uni-Ax, both from the company Mapei S. p.A. In order to improve the adhesion quality of the FRP-timber joint [18], Mapewood® Primer was applied to the timber before reinforcement. To ensure an MC of 10 ± 2% for the timber during the entire manufacturing process, the epoxy resin Mapewrap® 21 was used for FRP-wood adhesion. The main characteristics of the FRP used are summarized in Table 1.

2.3. Glulam timber: Layouts and manufacturing

Once the poplar planks were selected as described in Section 2.1, they were randomly used for the elaboration of the glulam beams. A total of 56 beams were manufactured, divided into 7 different layouts. Layout 1 (only poplar glulam beams) was used as the control group. Table 2 and Fig. 2 summarize all the layouts. Comparison of the different layouts (L) allows one to evaluate: i) The improvement provided by the FRP with respect to only-poplar beams, by comparing L2-L7 with L1; ii) The influence of the type of FRP, by comparing L3 and L2; iii) The influence of the FRP thickness by comparing L4 with L2; iv) The influence of the position of the FRP, comparing L5 with L3; and v) The influence of double reinforcement at compression and tension sides, by comparing L3, L6 and L7.

Fig. 2 shows the general design of 2100 mm long glulam beams used as test specimens. As seen, the design included finger joints for the connection between lamellas of the same layer elaborated according to the standard [17]– Annex I.4. For gluing, the polyurethane resin PUR-20

Table 1
Main characteristics of the used FRPs.

	CARBOPLATE E200	MAPEWRAP C UNI-AX
Fiber orientation	Unidirectional	Unidirectional
Density (g/cm^3)	1.56	–
Specific weight (g/m^2)	–	300
Thickness (mm)	1.400	0.166
Resistant area per width unit (mm^2/m)	1400.0	166.6
Max. tensile stress (MPa)	3300	4830
Tensile elastic modulus (GPa)	200	230
Max. elongation (%)	1.4	2.0

Table 2
Glulam beams layout description.

Layout	Type of FRP	Position of FRP	Number of layers	Total thickness of FRP (mm)	Cross-section ratio (%)	Number of samples	Nomenclature
1	–	–	–	–	–	8	CH
2	Fabric	Bottom	1	0.166	0.16	8	CFB
3	Lamella	Bottom	1	1.400	1.37	8	CLB
4	Fabric	Bottom	2	0.322	0.32	8	CF2B
5	Lamella	Top	1	1.400	1.37	8	CLT
6	Fabric	Top	2	0.322	0.32	8	CF2T
7	Fabric	Bottom + Top	2 + 2	0.322 + 0.322	0.64	8	CF2BT

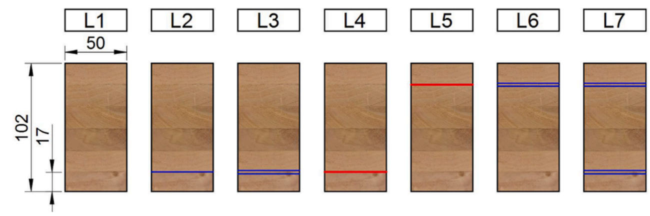

Fig. 2. Glulam layouts. Blue: FRP fabric. Red: FRP lamella. Distances in mm. (For interpretation of the references to colour in this figure legend, the reader is referred to the web version of this article.)

Bakar® structural adhesive was used. A pressure of 10 N/mm^2 was applied, as the length of the finger was 15 mm. After curing, the lamellas were mechanized to their final thickness, 17 mm.

The gluing process between different layers was performed according to the standard [17]– Annex I.5. Since the design of the glulam beams was set for Classes 1 or 2, the pith of the lamellas was orientated to the same side (upwards). The elaboration process was divided into four phases: i) Gluing the lamellas of the main timber section using the Bakar® PUR-20 resin (400 g/m^2); ii) Application of the primer (200 g/m^2); iii) Application of the FRP reinforcement, using 320 g/m^2 of epoxy resin; and iv) Gluing the external lamellas. During the entire manufacturing process, the moisture content of the timber was controlled, giving an average value of 11 ± 1%. After final curing, the beams were sawed at a final cross-section of 50 × 102 mm^2 and a length of 2100 mm (Fig. 3).

2.4. Non-destructive resonance test (NDT)

2.4.1. General description of the test

Non-destructive transversal resonance tests (NDT) entailed placing the samples on two elastic supports in edgewise orientation and using a timber hammer as the impact tool (see Fig. 4). A t.bonne MM-1 Thomann microphone was used to capture the elastic wave and convert it to a signal, which was recorded by a Picoscope® 4424 oscilloscope with 80 Ms/s of maximum sampling frequency. The BING program (*Beam Identification by Non Destructive Grading,* [19]) was used to obtain the transversal modulus of elasticity (MoE$_{dyn}$). This program is based on the theory proposed in [20] and relies on the flexural resonance frequency and the Timoshenko bending theory to determine the dynamic MoE and the shear modulus in free-free boundary conditions. Furthermore, [20] proposes the following first order solution for the motion of a resonance beam:

$$\frac{MoEdyn}{\rho} = \frac{MoEdyn}{KG} \cdot x_n + y_n \tag{1}$$

where MoE_{dyn} is the transversal dynamic MoE in edgewise position, ρ is the specimen density, K is the shear factor with a value of $K = 5/6$ for a rectangular cross-section, G is the dynamic shear modulus and x_n and y_n are parameters dependant on the vibration mode. According to [20], the maximum relative errors of MoE$_{dyn}$ and G respectively remain <5% and 8%, considering a length-to-depth ratio between 10 and 20 (in our case L/h was set as 20).

2.4.2. Resonance tests before the FRP application (Phase 1)

The elaboration process for the reinforced layouts (2–7) was divided in two phases:

-Phase 1, in which the main timber section of the beam was manufactured. After this phase, a NDT was performed separately upon the main glued section (ms) and upon the remaining non-glued lamellas (l) to obtain the MoE$_{dyn,ms}$ and MoE$_{dyn,l}$, respectively. By means of the Parallel Axes Theorem (Section 2.4.4), the combined dynamic modulus for each beam without reinforcement can be obtained for each particular beam (named as MoE$_{dyn,c}$). See clarifications in Fig. 5. More precisely,

$$MoE_{dyn,c} = \frac{MoE_{dyn,ms} \bullet I_{ms} + A_{ms} \bullet MoE_{dyn,ms} \bullet y_{ms}^2}{I_c} + \frac{MoE_{dyn,l} \bullet I_l + A_l \bullet MoE_{dyn,l} \bullet y_l^2}{I_c} \tag{4}$$

where I$_{ms}$ and I$_l$ are the second moments of inertia with respect to the sample axis, A$_{ms}$ and A$_l$ are the cross-sections, and y$_{ms}$ and y$_l$ are the distances from the combined neutral axis to the neutral axis of each part, respectively of the main section and the remaining lamella (s). I$_c$ is the combined second moment of inertia.

-Phase 2: After gluing the reinforcement and the external lamella(s), a NDT was performed, giving the dynamic modulus of the whole beam (MoE$_{dyn}$).

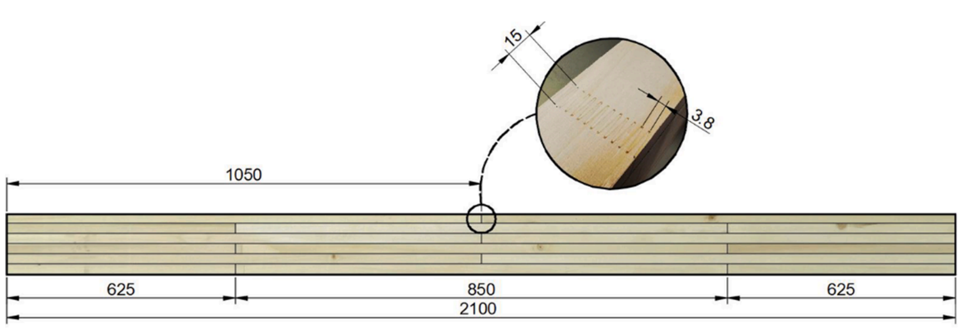

Fig. 3. General design of glulam beams. Distances in mm.

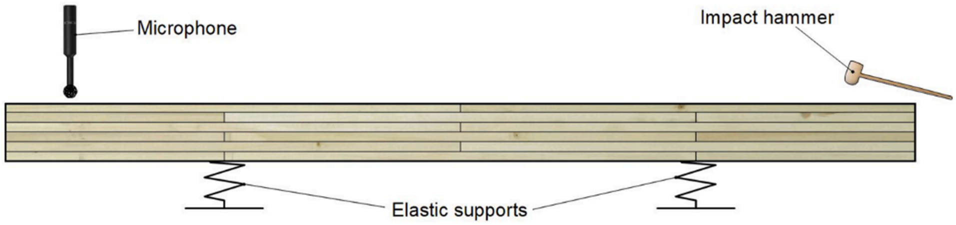

Fig. 4. General arrangement of the non-destructive resonance test.

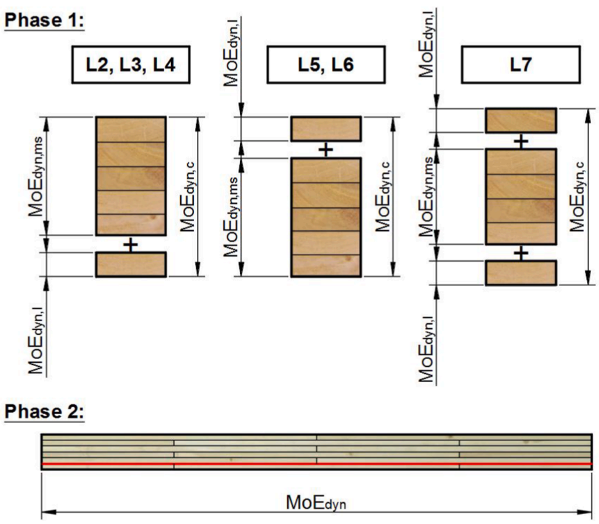

Fig. 5. NDT procedure for Phases 1 and 2 to obtain the $MoE_{dyn,c}$ and MoE_{dyn}.

2.5. Ductility

In order to obtain the ductility ratio, the elastic and the ultimate limit were defined according to [21]. They are represented in Fig. 6. This procedure can also be used to obtain the curvature ductility.

When plastification occurs, the force–displacement and moment–curvature relations become non-linear, hence essential for a proper estimation of the limits of the elastic and plastic range. As a geometric method to identify the limit between the elastic and plastic ranges, the use of two auxiliary lines is required (Fig. 6-left): i) Green dashed line, whose slope (tan(α)) was obtained as between 10% and 40% of the maximum load ($0.1F_{max}$ and $0.4F_{max}$); and ii) Red dashed-dotted line, tangent to the force–displacement curve, where the slope is equal to tan β = (1/6 tan α). Hence, the geometric intersection of these two lines defines the yielding point (F_y) and its corresponding displacement (δ_y). The ultimate displacement, $\delta_{u(B)}$, was established as the displacement when the load decreases by 20% (point B) after reaching its maximum value. If this drop was not reached, this value was set as the last load value achieved ($\delta_{u(A)}$).

However, due to the reinforcement, some layouts still afford bending capacity up to collapse even when the bottom layer has already failed. In other words, reinforcements lend ductility to the whole element. Taking this fact into account, two different displacement ductility ratios can be computed.

The same procedure can be applied to derive the ductility ratio based on the moment–curvature relationship, bearing in mind that the ductility ratio can be evaluated until bottom layer failure, which is directly related with the drop in the force–displacement relation.

In order to achieve practical applicability in line with the experimental results, two different approaches were considered (Fig. 6-right): one corresponding to the engineering design side, the other pertaining to structural safety. Therefore, for the specimens exhibiting successive drops in the force–displacement relationship, the ultimate displacement for the engineering design considerations would correspond to the first drop in the load–displacement relation (δ_{ue}), while for safety considerations, the ultimate displacement corresponds to the ultimate load prior to total collapse (δ_{us}). As mentioned above, moment–curvature ductility only provides an estimation of ductility corresponding to the engineering side. In order to automate this process and to provide a precise estimation of the ductility index for all the approaches, a versatile script was developed —employing Python programming language— considering the relationships of: i) displacement ductility – engineering design, $\mu_{\delta,ed}$ (Ec. 5); ii) displacement ductility – structural safety, $\mu_{\delta,ss}$ (Ec. 6); and iii) moment–curvature – engineering design, $\mu_{\chi,ed}$ (Ec. 7)

$$\mu_{\delta,ed} = \frac{\delta_{ue}}{\delta_y} \tag{5}$$

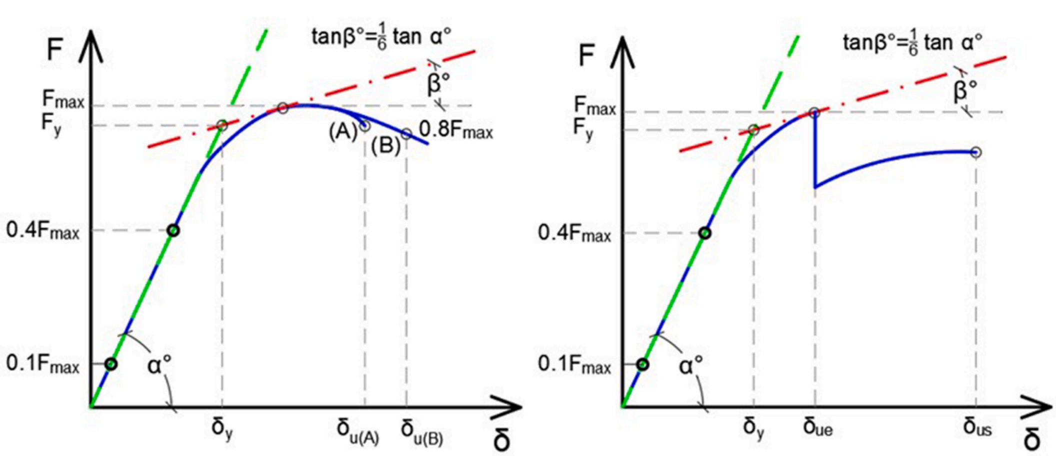

Fig. 6. Procedure to determine the ductility ratio in terms of displacements. F is the applied force and δ is the vertical deflection. Left: Theoretical approach; Right: Approach considered in this study.

$$\mu_{\delta,ss} = \frac{\delta_{us}}{\delta_y} \quad (6)$$

$$\mu_{\chi,ed} = \frac{\chi_{ue}}{\chi_y} \quad (7)$$

where δ_{ue} and χ_{ue} are the displacement and curvature at the maximum load for the engineering design, respectively; δ_{us} is the ultimate displacement for structural safety; and δ_y and χ_y are respectively the displacement and curvature at the yielding point.

2.6. Bending test

All the specimens were subjected to a 4-point bending test until failure, according to the standard [22]. Loading was applied at a controlled displacement rate of 8.7 mm/min. The tests were carried out with a machine from the company CONTROLS S.A., model S-110, with one electrical actuator having a maximum capacity load of 100 kN. The distance between supports was set as 1920 mm, while the distance between points of load application was 612 mm (Fig. 7). The strains were measured using four strain gauges (K-CLY-4 series from HBM) placed at the mid-span of the beam. The top and bottom strain gauges measured the compression and tensile strains, respectively; lateral strain gauges registered the strains at 1/4 of the total height of the beams. In order to avoid undesirable strain effects near the finger joint, top and lateral strain gauges were slightly displaced (15 mm). The objectives of the lateral gauges were: i) To determine whether the beam began to twist during the test; and ii) To obtain the experimental position of the neutral axis. By using the bottom strain gauge, the static modulus of elasticity (MoE_s) was obtained as the slope of the stress–strain relationship between 10% and 40% of the maximum stress. The maximum stress was computed with the bending theory at the mid-span, i.e.

$$f_m = \frac{3aP_{max}}{bh^2} \quad (8)$$

where, P_{max} is the maximum load (N), a is the distance between the load point and the nearest support (mm), b is the width of the beam (mm) and h^2 is the depth of the beam (mm). A LVDT was placed at the center of the beam to register the global modulus of elasticity ($MoE_{m,g}$) as stated by standard UNE-EN 408:2011 + A1:2012, comparable with the MoE_s.

2.7. Statistical analysis

Non-parametric Kruskal-Wallis tests were run by means of the package Statistix v.9® to determine the statistical differences among all the beam layouts.

3. Results and discussion

Fig. 8 shows the stress–deflection curves for all the samples of each particular layout. Two clear behaviors are identified —ductile and brittle. The ductile behavior is observed for the layouts with reinforcement at the tension layer (L2, L3, L4, and L7), whereas brittle behavior is seen only for the layouts having reinforcement at the compression layers (L5 and L6) or the control case without reinforcement (L1). Reinforcement at the tension layers lends the beam a high capacity to bear tensile stress. Consequently, the stress in the compression area of the timber is also increased, producing plastic deformations, introducing a non-linear behavior at an intermediate loading rate. As the plastic deformations increase, the active area in the elastic range is reduced. Tensile stresses therefore increase until the failure of the beam under tension.

Table 3 summarizes the results of the three ductility parameters defined in Section 2.5. Fig. 9 reflects the improvement (%) of these parameters compared with control layout L1. Fig. 10 offers an example of the typical failure patterns for one specimen of each particular layout. The CLB layout showed the highest improvement in terms of ductility (statistical class A for all three approches), with respective increases of 47% and 30% for engineering design and moment–curvature evaluations. Moreover, this layout provided a secondary improvement related to structural safety, around 107%. This is closely followed by the CF2B layout, giving important improvements of 26% – 115% for all three approaches (statistical class A). For the CFB layout, improvement ranges between 6% and 48% due to the thinner fabric layer, hence a statistical class between A and C. The main difference between the CFB and CF2B layouts is tied to the length of the elastic range and its corresponding slope. The CFB layout showed the shortest elastic range, with a relatively reduced slope due to the low value of the elasticity modulus. Owing to the thin fabric layer, the CFB specimens exhibited several premature failures at the bottom side (see Fig. 10). As the thickness of the reinforcement increased, a significant improvement in the elastic range is observed, along with a steeper slope. In such a case, the highest ductility is achieved for the structural safety side, because after failure of the bottom layer, the deflection is directly related to reinforcement stiffness. The CF2B and CLB layouts revealed a similar trend in the stress–deflection relation, yet there is a substantial difference regarding the respective yield points: the yielding range started sooner for the CF2B layout, providing the highest safety ductility, characterized by a smaller elastic range than that of the CLB layout. As seen in the fracture patterns (Fig. 10), these specimens have a deformed shape, the significant plastic deformation at the compression area being a consequence of the specimeńs high ductility.

For the CLT and CF2T layouts, decreasing ductility is clearly observed, identified through a straight linear variation of the stress–deflection relation; meanwhile, a clearly elastoplastic behavior is seen for layouts with reinforcement at the tension layers. Thus, the elastic range is shared by the layouts with brittle and ductile behavior. The most representative elastic range is that of the CLT specimen, exhibiting a steep slope and a wide elastic range without plastic deformation. The fracture patterns (Fig. 10) offer no evidence of plastic deformation for either the CLT or the CF2T layout. Such behavior can be attributed to the reinforcement at the compression layers, which impedes plastic behavior. The behavior becomes brittle because the tensile

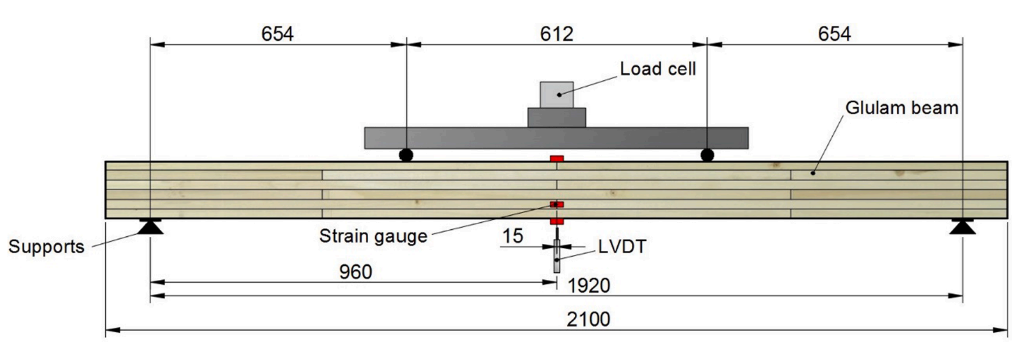

Fig. 7. Four-point bending test set-up. Distances in mm.

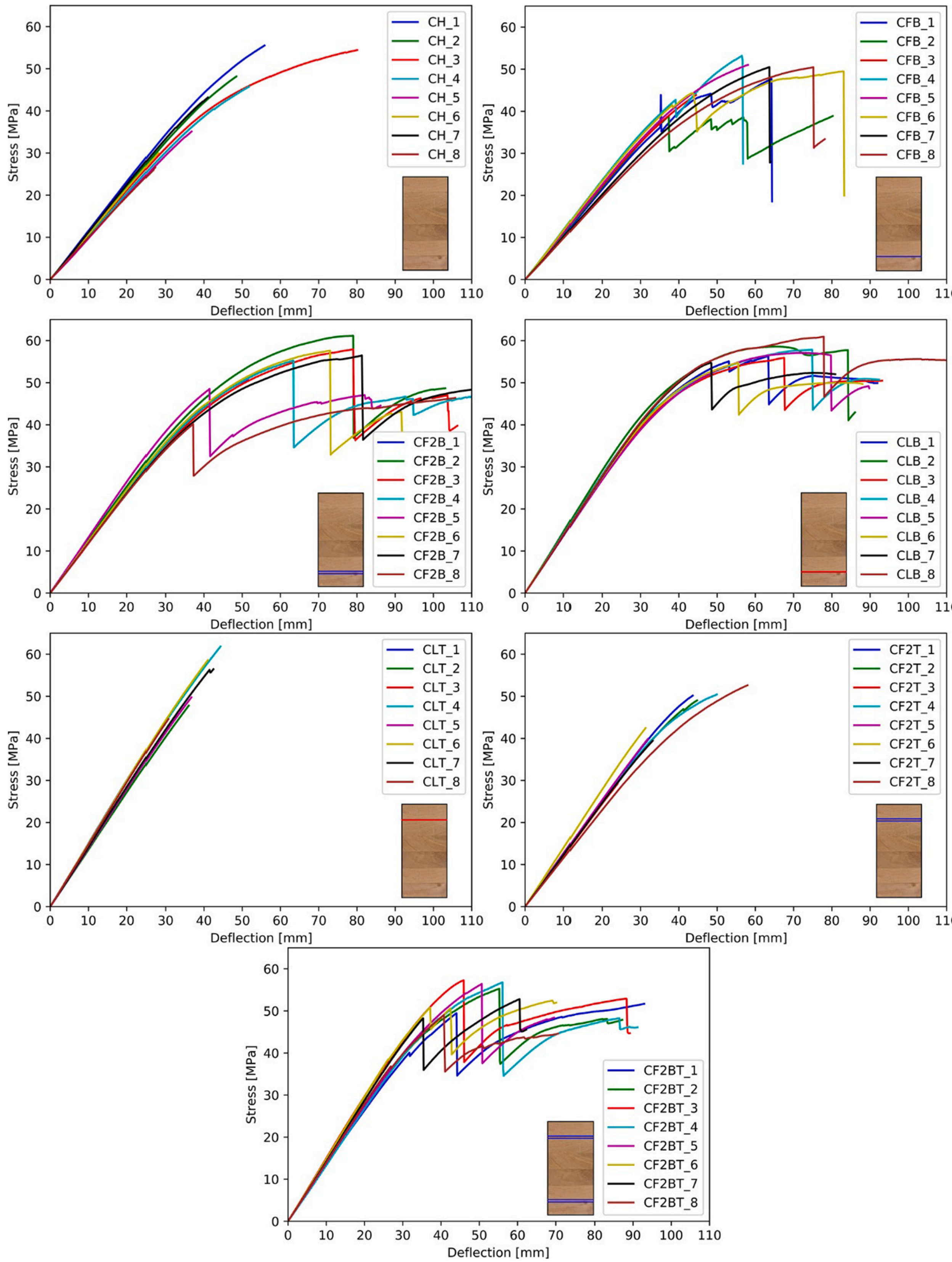

Fig. 8. Stress-deflection relations.

Table 3
Mean values, covariance (%) and statistical class for: force–displacement ductility parameters (structural safety and engineering design), and moment–curvature ductility.

Layout	Force-displacement (Structural safety) $\mu_{\delta,ss}$	Force-displacement (Engineering design) $\mu_{\delta,ed}$	Moment-curvature $\mu_{\chi,ed}$
CH	1.20 ± 20 BC	1.20 ± 20 BC	1.17 ± 16 AB
CFB	1.77 ± 23 ABC	1.27 ± 15 ABC	1.27 ± 17 AB
CF2B	2.58 ± 12 A	1.61 ± 19 AB	1.47 ± 16 A
CLB	2.48 ± 9 A	1.76 ± 17 A	1.53 ± 12 A
CLT	1.06 ± 2 C	1.06 ± 2 C	1.05 ± 2 B
CF2T	1.14 ± 11 BC	1.14 ± 11 BC	1.11 ± 12 B
CF2BT	2.19 ± 12.81 AB	1.26 ± 11 ABC	1.19 ± 17 AB
Kruskal-Wallis test	$F = 39.6$ $p < 0.05$	$F = 11.9$ $p < 0.05$	$F = 8.81$ $p < 0.05$

stress is only withstood by the poplar lamellas.

The CF2BT layout exhibited optimal behavior in both elastic and plastic terms, standing as reasonable improvement. In this case, the yield point is similar to cases CF2B and CLB, due to high stress concentration at the compression zone. One important feature observed in the experimental tests resides in the specimenś behavior during the second loading phase, after appearance of the first drop. The CF2B and CLB specimens exhibited excessive plastic deformation because the top area was plasticized, with high-stress concentrations being undergone only by the poplar lamella. The CF2BT layout behaved differently in the second phase, where a short elastic range is observed prior to the ultimate plasticization of the sections. As noted during the experiments, the high plasticizations can be traced to progressive debonding between poplar layers, and to cracks propagating along the beam (see Fig. 10).

Table 4 summarizes the results for the seven layouts regarding elastic moduli and maximum stress, including covariance and statistical results. Fig. 11 shows the improvement (%) of the static modulus and maximum stress when compared with control layout L1.

The selected poplar lamellas occupied a range of 6240–7882 N/mm^2. The range of mean values for the combined modulus $MoE_{dyn,c}$ was found to be 7286–8549 N/mm^2. These values are about 1000 N/mm^2 higher than those of the dynamic moduli of the single lamellas before gluing. In other words, the improvement can essentially be attributed to the gluing process (glue contribution), with a lesser influence of defects due to the finger joint manufacturing. The shear modulus of the specimens shows little variation, meaning that the reinforcement and gluing process hardly influence this mechanical parameter.

Regarding the MoE_{dyn}, the reinforcement improves stiffness, especially for the cases in which pultruded laminated is used (CLT and CLB) and two fabric layers are placed in the areas of tension and compression (CF2BT). Among these three layouts, no statistical differences were observed. Similarly, no statistically significant improvement was afforded by the fabric (one or two layers) placed only at the compression or the tension side, with respect to the control layouts CH.

The static modulus of elasticity (MoE_s) showed most noteworthy improvement when about 44% of pultruted laminate is placed at the tension side (CLB), with a clearly independent statistical class A as compared to the other layouts. This result is followed by an improvement of around 29% provided by the 2-layer carbon fabric at both compression and tension zones (CF2BT), characterized by the AB statistical class. The sections having reinforcement at the tensile zones bear the highest tensile stress, giving the highest improvement of the MoE_s, compared with the control section CH (C class), since the presence of the reinforcement increases stiffness in tension. It is worth mentioning that,

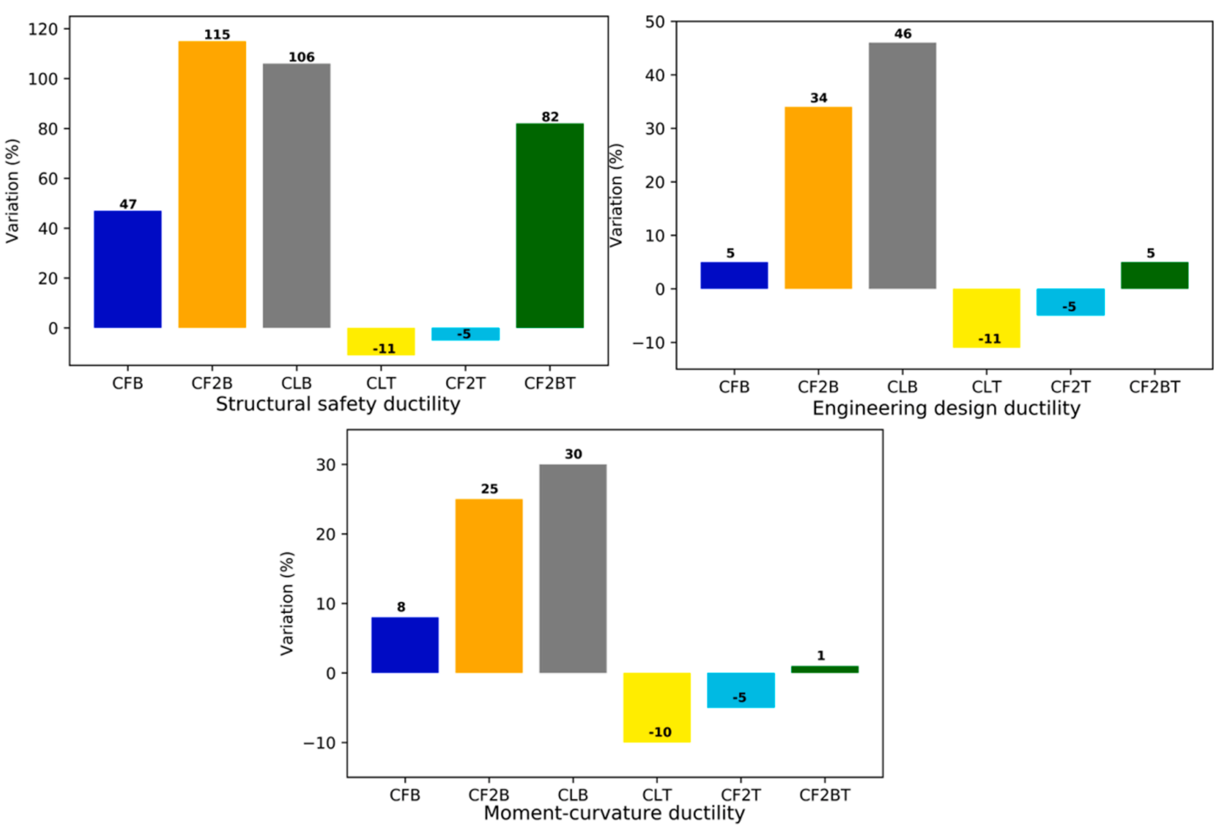

Fig. 9. Variations of the ductility parameters in % compared to the control CH layout.

Fig. 10. Failure patterns in bending.

Table 4
Mean values (N/mm^2), covariance (%) and statistical class of: $MoE_{dyn,c}$: dynamic combined modulus; G: Shear modulus; MoE_{dyn}: dynamic modulus; MoE_s: static modulus; $MoE_{m,g}$: global modulus without shear modulus (mean); MoE $_{m,g+G}$: global modulus of elasticity with shear modulus (mean); f_m: maximum stress.

Layout	$MoE_{dyn,c}$	MoE_{dyn}	G	MoE_s	$MoE_{m,g}$	$MoE_{m,g+G}$	f_m
CH	7586 ± 4 AB	7586 ± 4 B	866 ± 8 A	8146 ± 9 C	7615 ± 18 B	8033 ± 19 B	43 ± 26 B
CFB	7570 ± 5 AB	7926 ± 4 B	834 ± 9 A	8567 ± 14 BC	7865 ± 12 B	8300 ± 12 B	48 ± 10 AB
CF2B	7283 ± 4 B	8546 ± 5 AB	861 ± 7 A	9326 ± 9 ABC	8777 ± 11 AB	9317 ± 11 AB	55 ± 13 AB
CLB	761 ± 3 B	9656 ± 4 A	797 ± 8 A	11758 ± 8 A	10335 ± 8 A	11195 ± 8 A	57 ± 34 A
CLT	7901 ± 3 AB	10086 ± 5 A	847 ± 10 A	9535 ± 5 ABC	10885 ± 9 A	11805 ± 10 A	52 ± 12 AB
CF2T	7428 ± 3 B	8500 ± 7 AB	885 ± 7 A	9058 ± 14 BC	9140 ± 11 AB	9733 ± 13 AB	47 ± 17 B
CF2BT	8025 ± 5 A	9419 ± 5 A	864 ± 12 A	10525 ± 8 AB	1036 ± 19 AB	11200 ± 21 AB	54 ± 5 AB
Kruskal-Wallis test	$F = 8.77$ $p < 0.05$	$F = 42.9$ $p < 0.05$	$F = 1.06$ $p = 0.40$	$F = 10.8$ $p < 0.05$	$F = 9.18$ $p < 0.05$	$F = 10.1$ $p < 0.05$	$F = 6.08$ $p < 0.05$

due to the different behavior of timber under tension and compression, the maximum tension layer of the beam undergoes high tensile stress, meaning stress concentration in the reinforcement. Intermediate improvement is obtained for the CFB and CF2B, even when differences are not statistically relevant compared with the control layout (BC and ABC classes, respectively). Statistical tests also reveal some differences owing to increased carbon fabric thickness. Layouts CF2B and CLB showed relevant differences from a statistical viewpoint (ABC and A classes, respectively). A medium–high improvement is also obtained for some CLT and CF2T specimens, even though the reinforcement was at the compressive zone (11%-17%). The existence of the reinforcement would have increased the total stiffness of the specimen, and especially the modulus of elasticity at compression. Thus, the ratio between the modulus of elasticity in tension and the compression is reduced, acting as a homogeneous section (similar modulus at tension and compression). The reinforcement keeps the wood from developing plastic deformations at the compression area. Still, its behavior is perfectly linear, without a yielding range, due to the brittle behavior of the timber at tension. Finally, the CF2BT layout displayed a clear improvement in terms of the static modulus of elasticity (around 29%). It was observed that this layout reduces plastic deformation at the compression area, showing a proper behavior of the whole section up to failure, sustained by the stress–deflection relation and the failure pattern shown in Fig. 10.

Nearly the same tendency can be observed for the $MoE_{m,g}$ and $MoE_{m,g+G}$ elastic moduli. Moreover, differences are seen for the static and global moduli. This is mainly because the static modulus, MoE_s, was obtained by means of the strain gauge, taking the real strain at the mid-span of the beam. In turn, the global modulus was calculated according to the standard [22], in which the shear modulus is omitted. Yet the global modulus $MoE_{m,g}$ is highly influenced by the shear stresses, as opposed to the MoE_s, which is scarcely influenced by the shear but serves to measure the global deformation. The standard also gives a $MoE_{m,g}/G$ ratio equal to 16, which is far from the value of 9 obtained for the control layout. A direct application of the standard ratio is therefore not valid for all species. For CH beams, results demonstrate that when an appropriate value of G is considered ($MoE_{m,g+G}$), the difference between the static and global moduli decreases from 7% to just 1%. For the beams reinforced at compression with a pultruded laminate (CLT), the differences —even when G is applied— can be associated with the fact that measurement of G by NDT methods ignores the position of the

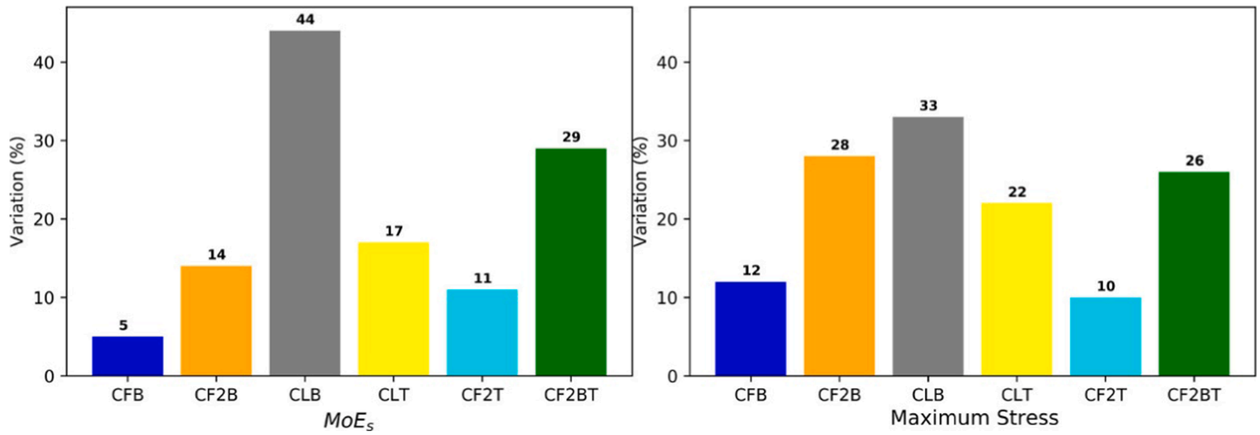

Fig. 11. Improvement of the static modulus of elasticity (left) and maximum stress (right) improvements respect to the control CH layout.

reinforcement in the destructive test.

In terms of the maximum stress (f_m), the highest improvement (around 33%) is also achieved when the pultruded laminate reinforcement is placed at the tensile zone. The influence of the reinforcement thickness is evident, meaning respective improvements from 12% to 28% for the CFB and CF2B layouts. Statistically, no differences are observed between the CF2B and CF2BT layouts, since the reinforcement has high performance under tensile stresses. Therefore, the reinforcement placed at the bottom side of the cross-section is the one that mostly contributes on the improvement of the maximum stress. Thus, for the same load level, in both cases the reinforcement in tensile area considerable reduces the stress in the bottom poplar lamella (maximum tensile) while the top reinforcement lightly reduces the tensile stresses at the bottom. The latter behaviour is evidenced by the CF2T layout (10% of improvement), where the reinforcement is only placed in compression, while the lower mid cross-section of the beam undergoes tensile stresses through the poplar lamellas. The CLT, with the pultruded laminate reinforcement placed at compression, achieves a significant improvement of roughly 22%, showing that even at compression, the thickness of reinforcement proves very relevant in terms of the maximum tensile stress.

A comparison of the dynamic moduli ($MoE_{dyn,c}$ and MoE_{dyn}) and the static modulus (MoE_s) is depicted in Figs. 12–14, representing all the samples of each layout (Figs. 12 and 13) or only the mean value for each particular layout. Figs. 12 and 13 show that the experimental points are basically grouped in clusters, each one associated with a particular layout. In greater detail, Fig. 12 clearly shows that all the points are distributed around a horizontal line, as $MoE_{dyn,c}$ represents the contribution of the poplar lamellas alone. It is clear that all the clusters corresponding to reinforcement layouts provide MoE_{dyn} values that are higher than the corresponding $MoE_{dyn,c}$, demostrating the improvement provided by reinforcement. Given the reasons expounded above, the clusters corresponding to CFB, CF2B and CF2T are very close to each other and very close to the CH control one, demostrating non-significant improvements from a statistical point of view. A pertinent example is the CF2B layout, where the $MoE_{dyn,c}$ of the section without reinforcement is 4.0 % below the control CH layout.

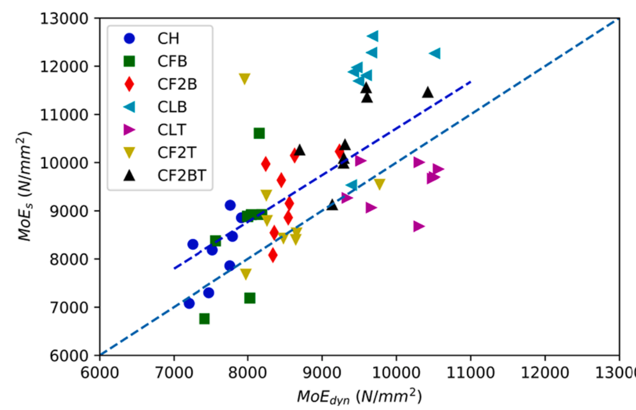

Fig. 13. Dynamic modulus of elasticity vs static modulus of elasticity for all specimens.

Fig. 12 displays a sample-by-sample comparison of the static and dynamic moduli. Once again, a clear difference can be seen between the CFB, CF2B and CF2T clusters, which are statistically very close to the control CH cluster, meaning no relevant improvements in stiffness; in contrast, the CLB, CLT and CF2BT clusters provide substantial improvement with respect to the control. Such behavior is likewise reflected in Fig. 14-left, where only the mean value of each particular layout is represented. In this case, though almost all the points are straightly aligned close to the 45° line —which would represent the optimum situation in which static and dynamic moduli are similar; that is, NDT and destructive tests providing the same results— the points for the layouts with pultruted carbon laminated lie beyond the linear behavior, demonstrating a clear influence of the type of reinforcement on the dispersion of results between the NDT and the destructive test. The difference is also highly conditioned by the position of the pultruted laminate, which would clearly influence the vibration patterns of the composite beam.

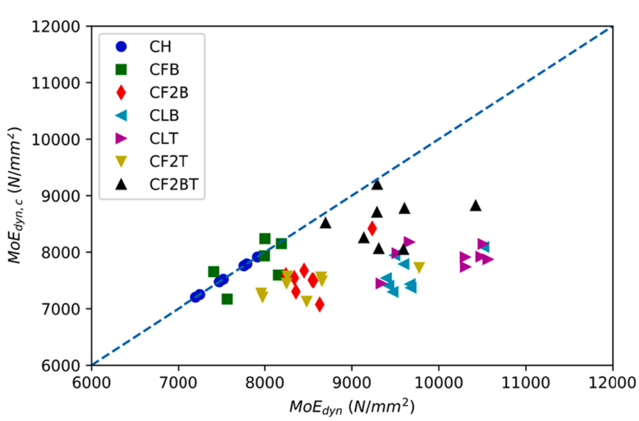

Fig. 12. Dynamic modulus of elasticity vs dynamic combined modulus for all specimens.

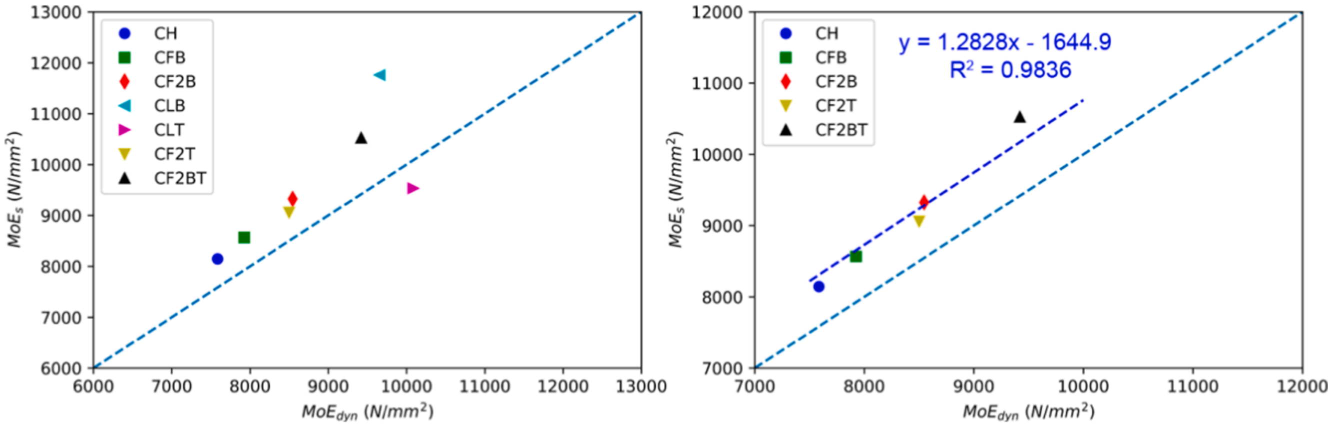

Fig. 14. Mean values of dynamic modulus of elasticity against static modulus of elasticity.

4. Conclusions

This paper demonstrates a clear influence of the position and the precise type of reinforcement along the timber cross-section upon the mechanical behavior of the whole element.

When one or two layers of carbon fabric are used (0.166 mm thickness each), either in the compression or the tension layer, only minor improvements in stiffness are obtained —no higher than 15%, and not significantly different from the control non-reinforced beams. The influence of fabric thickness on stiffness is limited, proving more relevant in the case of the maxium load, for which significant improvement is achieved when two fabric layers are used (around 28%).

For the case in which pultruted carbon laminate is used together with two layers of carbon fabric on both the compression and tension sides, significant improvements are obtained in terms of stiffness and strength (up to 44% and 33%, respectively, when reinforcement exists at the tension side). Improvement is lower when the reinforcement is used only on the compression side (17% and 22%, respectively).

A good correlation is observed between the dynamic and static moduli (non-destructive and destructive procedures), except when pultruted laminated carbon is used for reinforcement, in which case its position is clearly influential. This may be due to the higher mass ratio provided by the pultruted laminated as compared to the carbon fabric, conditioning the vibration pattern of the entire element. Nevertheless, this issue will be more deeply addressed in future work by using numerical simulations.

High values of ductility are obtained when the reinforcement is placed at the tension area (ductility values up 2.60). When reinforcement is placed only at the compression zone, a brittle behavior is observed, similar to that corresponding to the control case without reinforcement.

With the aim of taking this concept to a higher Technology Readiness Levels (TRL), two objectives will be addressed in future research: I) To elaborate and test specimens obtained from different plantations in the north and south of Spain; II) Employing finite element models (FEM), optimization and reliability techniques, high performance samples can be designed taking into account the statistical nature of the mechanical properties of the poplar timber materials."

Funding

This work has been possible thanks to the financial support of the COMPOP_Timber project "*Desarrollo de productos de ingeniería elaborados a base de tablones y chapas de chopo con inserciones de material compuesto para su uso en construcción*", BIA2017-82650-R.

CRediT authorship contribution statement

Francisco J. Rescalvo: Writing - original draft, Writing - review & editing, Conceptualization, Methodology, Investigation. **Cristian Timbolmas:** Writing - original draft, Investigation, Data curation, Validation. **Rafael Bravo:** Supervision, Writing - review & editing, Validation, Formal analysis. **Ignacio Valverde-Palacios:** Investigation, Resources. **Antolino Gallego:** Conceptualization, Supervision, Writing - review & editing, Validation, Funding acquisition.

Declaration of Competing Interest

The authors declare that they have no known competing financial interests or personal relationships that could have appeared to influence the work reported in this paper.

Acknowledgments

The authors gratefully acknowledge the LaBoMaP group of the Art et Métiers, Sciences et Technologies University for BING program support, MAPEI® S.A.U. for the supply of reinforcement, and Dr. María A. Ripoll at the IFAPA for harvesting work, timber characterization on standing trees and timber supply for the project.

Contribution of the authors

F.R.: writing, experimental work, experimental design; **C.T.:** writing, experimental work and data analysis and interpretation; **R.B.:** supervision, writing, data analysis and interpretation; **I.V.:** experimental support. **A.G.:** supervision, poplar timber, writing, and interpretation.

References

[1] M.H. Ramage, H. Burridge, M. Busse-Wicher, G. Fereday, T. Reynolds, D.U. Shah, G. Wu, L. Yu, P. Fleming, D. Densley-Tingley, J. Allwood, P. Dupree, P.F. Linden, O. Scherman, The wood from the trees: The use of timber in construction, Renew Sust Energ Rev. 68 (1) (2017) 333–359, https://doi.org/10.1016/j.rser.2016.09.107.

[2] F. Theakston, A feasibility study for strengthening timber beams with fiberglass, Can. Agric. Eng. 7 (1965) 17–19.

[3] R.E. Rowlands, R.P. Van Deweghe, T.L. Laufenberg, G.P. Krueger, Fiber-reinforced wood composites, Wood Fiber Sci. 18 (1) (1986) 39–57.

[4] T.G. Williamson, Fire performance of fiber reinforced polymer glued laminated timber. Proceedings 9th World Conference on Timber Engineering, 2006.

[5] Z.A. Martin, D.A. Tingley, Fire resistance of FRP reinforced glulam beams. Proceedings of World Conference on Timber Engineering, Whistler. 2000.

[6] R. Hernandez, J. Davalos, S.S. Sonti, Y. Kim, R.C. Moody, Strength and stiffness of reinforced yellow-poplar glued-laminated beams, Forest Products Laboratory. RP-554 (1997) 28.

[7] W. Luggin, K. Bergmeister, Carbon fiber reinforced and prestressed timber beams. Proceedings 2nd Int. PhD Symposium in Civil Engineering, 1998.

[8] Y.J. Kim, K.A. Harries, Modeling of timber beams strengthened with various CFRP composites, Eng. Struct. 32 (10) (2010) 3225–3234, https://doi.org/10.1016/j.engstruct.2010.06.011.
[9] W. Lu, Z. Ling, Q. Geng, W. Liu, H. Yang, K. Yue, Study on flexural behaviour of glulam beams reinforced by Near Surface Mounted (NSM) CFRP laminates, Constr. Build Mater. 91 (2015) 23–31, https://doi.org/10.1016/j.conbuildmat.2015.04.050.
[10] A.S. Ribeiro, A.M.P. de Jesus, A.M. Lima, J.L.C. Lousada, Study of strengthening solutions for glued-laminated wood beams of maritime pine wood, Constr. Build Mater. 23 (8) (2009) 2738–2745, https://doi.org/10.1016/j.conbuildmat.2009.02.042.
[11] S. Osmannezhad, M. Faezipour, G. Ebrahimi, Effects of GFRP on bending strength of glulam made of poplar (*Populus deltoids*) and beech (*Fagus orientalis*), Constr. Build Mater. 51 (2014) 34–39, https://doi.org/10.1016/j.conbuildmat.2013.10.035.
[12] H. Yang, W. Liu, W. Lu, S. Zhu, Q. Geng, Flexural behaviour of FRP and steel reinforced glulam beams: Experimental and theoretical evaluation, Constr. Build Mater. 106 (2016) 550–563, https://doi.org/10.1016/j.conbuildmat.2015.12.135.
[13] G.M. Raftery, A.M. Harte, Low-grade glued laminated timber reinforced with FRP plate, Composites: Part B 42 (4) (2011) 724–735, https://doi.org/10.1016/j.compositesb:2011.01.029.
[14] G.M. Raftery, C. Whelan, Low-grade glued laminated timber beams reinforced using improved arrangements of bonded-in GFRP rods, Constr. Build Mater. 52 (2014) 209–220, https://doi.org/10.1016/j.conbuildmat.2013.11.044.
[15] A. Jorissen, M. Fragiacomo, General notes on ductility in timber structures, Eng. Struct. 33 (11) (2011) 2987–12977, https://doi.org/10.1016/j.engstruct.2011.07.024.
[16] F.J. Rescalvo, C. Timbolmas, R. Bravo, A. Gallego, Experimental and numerical analysis of mixed I-214 poplar/*pinus sylvestris* laminated timber subjected to bending loadings, Materials 13 (2020) 3134, https://doi.org/10.3390/ma13143134.
[17] UNE-EN 14080:2013, Timber structures – Glued laminated timber and glued solid timber – Requirements.
[18] F.J. Rescalvo, A. Aguilar-Aguilera, E. Suarez, I. Valverde-Palacios, A. Gallego, Acoustic emission during wood-CFRP adhesion tests, Int J Adhes Adhes. 87 (2018) 79–90, https://doi.org/10.1016/j.ijadhadh.2018.09.007.
[19] Cirad. Non-destructive testing of wood. 2020. https://www.picotech.com/library/application-note/non-destructive-testing-of-wood.
[20] L. Brancheriau, H. Bailleres, Natural vibration analysis of clear wooden beams: a theoretical review, Wood Sci Technol 36 (4) (2002) 347–365, https://doi.org/10.1007/s00226-002-0143-7.
[21] UNE-EN 1995-1-1:2016, Eurocode 5: Design of timber structures – Part 1-1: General-Common rules and rules for buildings.
[22] UNE-EN 408:2011+A1:2012, Timber structures – Structural timber and glued laminated timber – Determination of some physical and mechanical properties.